Chapter 3

Single shot and speckle free reconstruction of orthogonal polarization modes with a tuneable beam displacer

3.1 Introduction

A coherent light source has been commonly used for a wide range of applications such as in wavefront shaping, interferometry, holography, microscopy, tomography, and metrology, to name a few [85]. However, propagation of coherent light in a medium with refractive index inhomogeneity, such as diffuser, fog, etc scrambles the wavefront and generates a coherent noise, also referred to as speckle [86]. Use of coherent optical systems becomes a challenging task in the presence of speckle due to masking and change in the desired signal content. In a generic case, the coherent beam interacts with the object and scattered light is analysed to reconstruct the information about the object. In spite of the common occurrence

of the speckle, a coherent laser is a preferred source due to its high monochromaticity, brightness and colour gamut. Therefore, it is desirable to devise a mechanism to either reduce the speckle patterns [86, 87] or provide an alternative approach to use the speckle patterns to extract useful information [24, 86, 88]. We want to utilize the randomness for imaging purposes instead of considering this as an obstacle. Imaging from the randomly scattered light and laser speckle is a challenging, yet practical, problem in a wide range of applications. When the object is obscured by the scattering media, both white-light imaging and conventional imaging methods are not suitable to provide useful information from the speckle. Hence, numerous methods have been proposed to investigate the issue of imaging through random scattering media [34, 51, 89, 90, 91, 92, 93, 94, 95, 96, 97]. Desired information can be recovered from the randomly scattered light with a priori information of the transmission matrix of the scattering medium [30, 98]. Adaptive optics techniques have also been proposed to deal with the issue of imaging through random scattering medium [99]. Available resources and new advancements in wavefront shaping with digital methods have significantly contributed to laser beam focusing and imaging through scattering medium [27, 100]. Randomness of the light has also been used for wavefront sensing [101, 102], and in non-line of sight imaging [103]. Spatial and spectral control using meta optics has become a new trend for wavefront shaping [104], and a metasurface diffuser has been designed for computational imaging [105]. Speckle produced by random scattering remains correlated within a range of small angular tilt in the incident beam and this feature is known as the memory effect [34, 37, 88]. This feature has been exploited to realize scattering media as a lens and in visualizing the object hidden behind the random scattering medium. Deconvolution in speckle correlation with iterative algorithms has been used to design and develop several new methods for seeing through scattering medium [106, 107]. Attempts have also been made to enlarge the field of view for imaging through scattering media with a speckle demixing approach [108] , adaptive

parameter in iterative algorithm [109], and by coupling polarization modes of the light [43]. Another imaging technique for high resolution has been reported by utilizing the shower curtain effect [110] . Learning based methods have also been used for imaging through random scattering media [92, 111, 112]. Other important methods for imaging through random scattering media are auxiliary [113] and structured light [114, 115] etc. On the other hand, holographic methods have long been applied for wavefront correction [116] and to improve images through refractive index inhomogeneity [117]. Moreover, holographic techniques are free from iteration and convergence issues. In the past, two important holographic methods were developed by Goodman et al [118] and Kogelnik and Pennington [119] for imaging through scattering medium. Singh et al proposed a holography technique for looking through a diffuser with a digital holography approach [120]. This technique uses imaging optics to take advantage of the digital holography with incoherent addition of speckle patterns using a rotating diffuser. In recent communications, alternative methods have been developed for imaging through random scattering medium by applying the spatial ergodicity and stationarity of the random light to retrieve speckle free images [39, 40, 121, 122]. These techniques rely on the common analogy between the optical field and complex coherence function and make use of two central results of the coherence optics; namely the van Cittert–Zernike theorem and the Hanbury Brown Twiss (HBT) approach. Different experimental geometries such as off-axis, phase shifting, polarization guiding, etc have been used to realize holography with the HBT approach [121]. Akhlaghi and Dogariu have demonstrated another approach for single-shot coherent noise suppression by spatial interferometric heterodyning [123]. This method operates under very low signal to noise ratio(SNR) situations and separates the spectral components of the signal and noise. Such initiatives for a polarized object appear to not attract much attention except for some recent investigations in the context of ghost polarimetry [124, 125, 126], lensless stokes holography [127] and higher order stokes correlations [5],

etc. Polarization fluctuations in the random field affect the speckle contrast and degree of polarization. Over the past few years, significant attempts have also been made on characterization of polarization speckle, i.e. speckle with polarization fluctuations for imaging and characterization of the light [42, 128, 129, 130].

In this chapter, we present and demonstrate a new technique for parallel and speckle free recovery of the orthogonal polarization modes from the randomly scattered light. Propagation of coherent and polarized light through a scatterer generates a speckle pattern with polarization variation. Because the incident light is monochromatic and the scattering surface is static, a spatially fluctuating random field is generated. In order to implement a parallel recovery of the orthogonal polarization modes of the light from random pattern, we designed a triangular polarization Sagnac interferometer assembly with fine tuning of the mirror for lateral separation of the orthogonal polarization components. Due to propagation of light through the diffuser and high angle scattering, it is hard to isolate the speckle patterns of the orthogonal polarization components at the recording plane by a fixed angle Wollaston prism or beam displacer. Therefore, controlled and variable separation of speckles of the orthogonal polarization components is desired for parallel detection of the orthogonally polarized speckle patterns and estimation of the two-point intensity correlations from a single measurement. A phase loss problem is a very common occurrence in intensity correlations, and attempts have been made to overcome this issue [37, 39, 51]. In order to avoid phase recovery issues in our proposed scheme, we use an edge referencing approach for holography with the coherence waves in intensity correlations. An edge reference means a reference point in the vicinity of the object itself rather than a separate reference beam as used in many different off axis holographic optical setups. Edge referencing can be achieved by different means [131, 132, 133]. Moreover, our experimental approach is free from iterations, and capable of providing a speckle free

image. The following discussion includes a thorough theoretical justification and the associated experimental studies.

3.2 Theory

Consider a monochromatic and transversely polarized electric field with orthogonal polarization components, $E_x(\rho,t)$ and $E_y(\rho,t)$, where ρ is the spatial position vector, and t represents the time. For convenience, t is ignored for further calculations. The electric field vector is represented by $E_p(\rho,t)$, where $p = x,y$ in suffix represents the orientation of electric field vectors along horizontal and vertical directions. When a coherent monochromatic light propagates through a diffuser, it generates a laser speckle. In the proposed scheme, the object is obscured by the diffuser. The orthogonal polarization components at the diffuser plane are represented as,

$$E(\rho) = \begin{pmatrix} E_p(\rho) \\ E_q(\rho) \end{pmatrix} exp(i\phi(\rho)) \tag{3.1}$$

where $\phi(\rho)$ is the random phase introduced by the diffuser. A diffuser is considered to create a random phase uniformly distributed on the interval $[-\pi,\pi\ ]$ which creates a Gaussian speckle pattern at the observation plane. Scattering from the diffuser makes a random fluctuation in the propagation. Consider the propagation of light beam from the scattering plane to an observation plane r located at a distance z as shown in Fig. 3.1. The propagated field at the observation plane is represented as,

$$E_p(r) = \int T_p(\rho)G(r,\rho)E_p(\rho)d\rho \tag{3.2}$$

where r is the spatial coordinate at the observation plane, $T_p(\rho)$ represents the orthogonal components of the object and $p = x,y$ represents orthogonal modes. $G(r,\rho)$ is the

propagation kernel [7] and is given by,

$$G(r,\rho) = \frac{exp(ikz)}{i\lambda z} exp(ik\frac{|r|^2+|\rho|^2-2r\rho}{2z}) \tag{3.3}$$

where $k = \frac{2\pi}{\lambda}$ and λ are the wave number and wavelength of light, respectively. The observation plane at a distance z from the scattering plane is considered to be within the Fresnel regime. Using equation (3.3) in equation (3.2), the orthogonal polarization components are represented as,

$$E_x(r) = A\int exp(ik\frac{|\rho|^2-2r.\rho}{2z})E_x(\rho)T_x(\rho)d\rho \tag{3.4}$$

$$E_y(r) = A\int exp(ik\frac{|\rho|^2-2r.\rho}{2z})E_y(\rho)T_y(\rho)d\rho \tag{3.5}$$

where $A = \frac{exp(ikz)}{i\lambda z} exp(ik\frac{|r|^2}{2z})$. Considering the source, a combination of object and an edge reference, as shown in Fig. 3.1, the complex field at the observation plane is expressed as,

$$E_p(r) = E_p^1(r) + E_p^2(r) \tag{3.6}$$

where $E_p^1(r)$ and $E_p^2(r)$ are the two independent sources, for e.g. in Fig. 3.1, one term is due to the object i.e. number '2', and the other is the edge reference contribution. This edge point introduces an independent randomness from the object region. Depending on the type of incident polarized light, coherent and polarized light propagation through the scatterer may cause polarization variation in the randomly scattered field. The term 'polarization speckles' refers to such a random field with spatially variable polarization that is useful for identifying the incident polarized light. The intensity at the observation plane is represented as,

$$I(r) = |E_x(r)|^2 + |E_y(r)|^2 \tag{3.7}$$

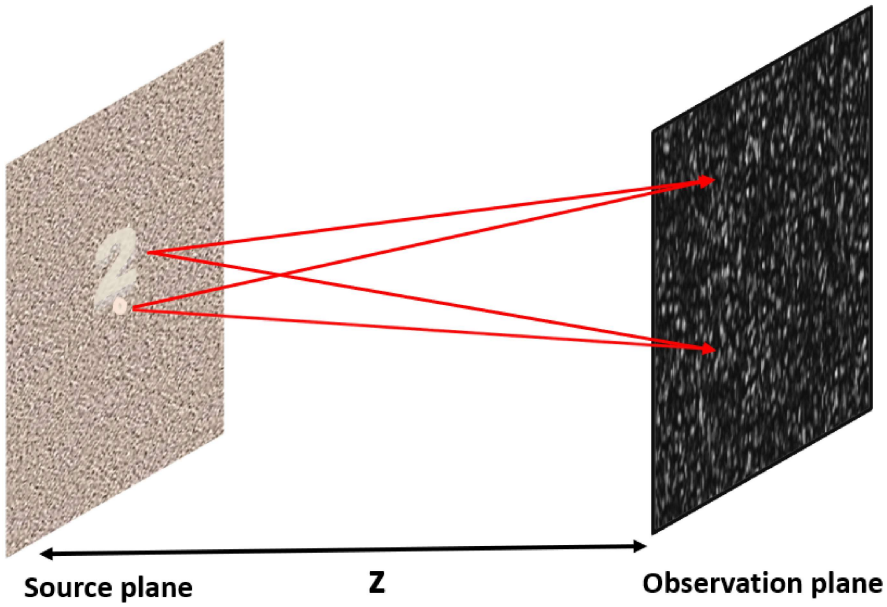

Fig. 3.1 Conceptual representation of speckle at arbitrary distance z

A two-point intensity correlation of the random field is $\langle I_p(r_1)I_p(r_2)\rangle = \langle E^*(r_1)E(r_1)E^*(r_2)E(r_2)\rangle$ where r_1 and r_2 are two spatial points at the observation plane. The intensity fluctuations from its mean value corresponding to the measured intensity is given by $\Delta I(r) = I(r) - \langle I(r)\rangle$, where parenthesis $<...>$ represents the ensemble average. A cross covariance $C(r_1, r_2)$ of intensity is stated as,

$$C(r_1, r_2) = \langle \Delta I(r_1)\Delta I(r_2)\rangle = \langle I(r_1)I(r_2)\rangle - \langle I(r_1)\rangle\langle I(r_2)\rangle \tag{3.8}$$

We use the concept of coherence wave interference for the vectorial light field to investigate the polarization speckles [40]. The cross covariance gives an interference of two coherence waves with an incident polarization state p, q and can be represented as,

$$C(r_1, r_2) = \sum_{p,q} |W_{pq}^1(r_1, r_2) + W_{pq}^2(r_1, r_2)|^2 \tag{3.9}$$

where $W_{pq}^{1}(r_1, r_2)$ and $W_{pq}^{2}(r_1, r_2)$ are the elements of coherence polarization matrix defined as $W_{pq}^{m}(r_1, r_2) = \langle E_p^*(r_1) E_q(r_2) \rangle$, $m = 1, 2$ and $p, q = x, y$. Term $C(r_1, r_2)$ is the cross-covariance of intensities which is given by the interference of these two coherence waves arising from the object and edge reference. A random field at the observation plane may show spatial polarization inhomogeneity due to coupling of randomly scattered two orthogonally polarized modes. Characterization of such random light with intensity correlations requires contribution of all four terms of the 2×2 coherence–polarization (CP) matrix as explained in equation (3.9) [45, 134]. However, the situation of a coherently illuminated object at the diffuser plane can be dealt with only two diagonal elements of the CP matrix by separating the two orthogonal polarization components at the observation plane, i.e. not allowing two orthogonal polarization modes to intermix at the recording plane [63, 135]. This is experimentally implemented in our work by design of a tuneable beam displacer (rather than a Wollaston prism). By estimating the intensity covariance distribution of an orthogonally polarized random field, it is possible to digitally reconstruct the complex coherence function from the recorded intensity and, through it, the orthogonal modes of the object. By estimating the intensity covariance distribution of an orthogonally polarized random field, it is possible to digitally reconstruct the complex coherence function from the recorded intensity and, through it, the orthogonal modes of the object.

$$C_{pp}(r_1, r_2) = \langle \Delta I_p(r_1) \Delta I_p(r_2) \rangle \tag{3.10}$$

The field at the observation plane is made up of contributions from the object and reference, two independent sources at the scattering plane as shown in Fig. 3.1. Using equation (3.6), the two-point intensity correlation due to contribution of object beam and reference beam,

can be given as,

$$\langle I_p(r_1)I_p(r_2)\rangle = \langle (E_p^1(r_1)+E_p^2(r_1))^*(E_p^1(r_1)+E_p^2(r_1)(E_p^1(r_2)+E_p^2(r_2))^*(E_p^1(r_2)+E_p^2(r_2)\rangle \tag{3.11}$$

where we choose two points, with one point fixed at $r_1 = r$ and the second point varied all over the speckle pattern i.e. $r_2 = r + \Delta r$. Making use of equations (3.4) and (3.5) in equation (3.11) and finally putting in equation (3.8) provides the cancellation of the common phase curvature $exp(ik\frac{|u|^2}{2z})$ in equations (3.4) and (3.5). Moreover, due to independent randomness of source and edge reference, the cross correlation terms get cancelled which leads to the contribution of only two complex coherence functions i.e. one from object and another from edge reference. By applying the Gaussian moment theorem under the consideration of Gaussian statistics [51] in equation (3.11), the fourth order correlation terms are expressed in second order correlations and we finally arrive at the following equation.

$$C_{pp}(r, r+\Delta r) = |W_{pp}^{1}(r, r+\Delta r) + W_{pp}^{2}(r, r+\Delta r)|^2 \tag{3.12}$$

From a non-stationary source, a stationary field is created at any arbitrary plane with $z > 0$, by combining the idea of coherence wave interference with intensity correlation [40]. The complex coherence function terms given in equation (3.12), i.e. two diagonal elements of coherence polarization matrix for two different orthogonal polarization components p, can be expressed as,

$$W_{pp}(r_1, r_2) = \langle E_p^*(r_1)E_p(r+\Delta r)\rangle \tag{3.13}$$

Using equations (3.4) and (3.5) in equation (3.13) and applying the spatial averaging, the two-point complex coherence is represented as,

$$\begin{aligned} W_{pp}(r, r+\Delta r) = \iint & E_p^*(r_1) T_p(r_1) E_p(r_2) T_p(r_2) \\ & \times \exp\left(\frac{-ik(|\rho_1|^2 - |\rho_2|^2)}{2z}\right) \exp\left(\frac{-ik(\Delta r.\rho_2)}{z}\right) \\ & \times \left[\int \exp\left(\frac{-ik(\rho_2 - \rho_1).r}{2z}\right)\right] dr d\rho_2 d\rho_1 \end{aligned} \tag{3.14}$$

Making use of the relation,

$$\int \exp\left(\frac{-ik(\rho_2 - \rho_1).r}{2z}\right) dr = \delta(\rho_2 - \rho_1) \tag{3.15}$$

and considering $\rho_2 = \rho_1 = \rho$, equation is transformed to,

$$W_{pp}(\Delta r) = \int I_{pp}(\rho) \exp\left(\frac{-i2\pi\Delta r.\rho}{\lambda z}\right) d\rho \tag{3.16}$$

where $I_{pp}(\rho) = |T_p(\rho)|^2$ represents intensity of the orthogonally polarized source at the scattering plane under the assumption of uniform illumination at the source. It should be noted that in equation (3.16) the complex coherence function depends only upon the difference between two coordinates i.e. Δr rather than the individual location of r_1 and r_2. Using equation (3.16), in equation (3.12), the four terms coming from the right hand side give rise to the formation of correlation fringes in the intensity correlation. Here the correlation fringes are formed by the interference of the two coherence waves; one from the object and other from the edge reference as shown in equation (3.16). Therefore, equation (3.12) can be expressed as,

$$C_{pp}(\Delta r) = |W_{p_p}^{1}(\Delta r)|^2 + |W_{p_p}^{2}(\Delta r)|^2 + W_{p_p}^{1*}(\Delta r) W_{p_p}^{2}(\Delta r) + W_{p_p}^{2*}(\Delta r) W_{p_p}^{1}(\Delta r) \tag{3.17}$$

where $W_{pp}^{1}(\Delta r)$ and $W_{pp}^{2}(\Delta r)$ are the coherence functions corresponding to the object and the edge reference, respectively and $p = x, y$. It should be noted that equation (3.17) is an interference of the coherence waves rather than the optical complex fields. A Fourier transform of equation (3.17) generates four terms and helps to provide the reconstruction of the desired object by Fourier filtering and processing. The first two terms in the Fourier space represent the unmodulated term (DC term). On the other hand, the 3rd and 4th terms represent the modulation term arising due to spectrums of complex coherence of the object and edge reference as discussed in equation (3.16). The separation between the DC term and the desired spectrum is affected by an off-axis location of the reference source with respect to the object as described by equation (3.16). The Fourier transform of correlation fringes of the orthogonal polarization components are not distinguishable, i.e. in overlapping condition in the frequency space. Therefore, in order to distinguish the Fourier spectrum of correlation fringes of the orthogonal components $p = x, y$ in a single measurement and implement a parallel recovery of the orthogonal modes, we developed a technique to spatially separate and record the speckle patterns of the orthogonal polarization modes. This helps to parallelly retrieve the correlation fringes for both orthogonal polarization components and get their Fourier spectrum using equation (3.17).

3.3 Experiment

An experimental setup of the proposed scheme is shown in Fig. 3.2(a). A monochromatic laser beam (wavelength 633 nm, Thorlabs, Model No. HNL 150 l) is spatially filtered by a spatial filter assembly, and collimated by using a biconvex lens L1 with focal length f = 200 mm as shown in the experimental geometry. A half wave plate (HWP) is used to orient the input beam polarization into 45° linearly polarized light. This light beam illuminates the OHP (overhead projector) transparency T placed close to the diffuser (Thorlabs, N-BK7, Model no. DG20-120-MD). This diffuser obstructs the object from the observation

plane. Two coherence waves, one arising from object which is obscured by a random media and other from an edge reference, propagate to an arbitrary distance z. However, the polarization speckles for two orthogonal polarization components get mixed and are non-separable, i.e. $I(r) = I_x(r) + I_y(r)$. In order to separate the orthogonal polarization components, one may employ a fixed angle Wollaston prism or beam displacer. However, these devices are of limited use in the case of randomly scattered light due to high scattering and inter mixing of random patterns. Therefore, it is necessary to design a variable beam displacer for separation of orthogonally polarized speckle patterns. Here, we realize this objective by designing a polarization sensitive Sagnac setup capable of providing tuneable separation of the speckle patterns of the orthogonal polarization components at the observation plane. A Sagnac geometry consisting of two mirrors (M1 and M2) and one polarizing beam splitter (PBS) is used to spatially separate the speckle of the orthogonal polarization components and hence simultaneously reconstruct the polarization components of the object. A PBS splits the speckle pattern into two orthogonal polarized components. The horizontal component of light transmits through the PBS and is directed towards the observation plane by mirrors M1 and M2. The Sagnac geometry is a common path interferometer, where both the beams travel nearly equal distances and after travelling through the interferometer, they both come out the PBS moving towards the detector. An imaging lens of focal length 100 mm is used to image the orthogonal polarization speckles at the detector plane. The lens L2 is placed at a distance 2f, i.e. 200 mm, from the observation plane (shown by the green arrow in Fig. 3.2(a)), and the detector is placed at same distance 2f from lens L2, forming a 4f system. A light field from the source plane propagates to an observation plane (shown by green arrow in Fig. 3.2) located at a distance of 100 mm, and this plane is imaged by lens L2 at the camera plane. The speckle field at the observation plane is imaged and recorded by (CMOS-Thorlabs, Model No. DCC3240C) camera with 1024 × 1280 pixels, and pixel size 5.4 μm. Separation of the speckle patterns

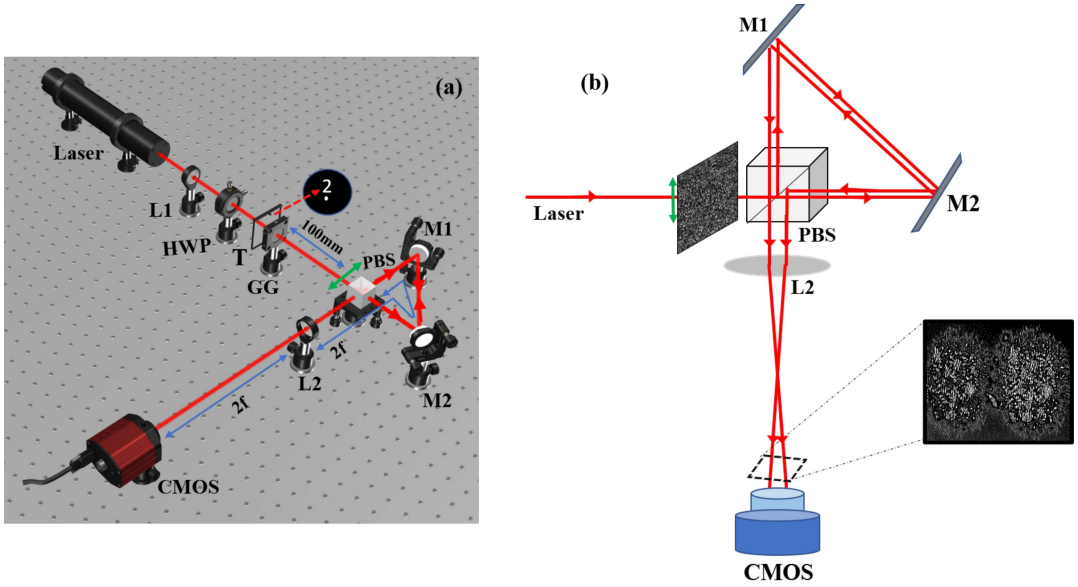

Fig. 3.2 (a) The experimental scheme of the proposed work, Ln(n = 1,2): lens, HWP: half wave plate, T: object with edge reference (shown by red dotted arrow), GG: ground glass, PBS: polarizer beam splitter, Mn(n = 1,2): mirrors, CMOS Camera: complementary metal-oxide semiconductor camera. The green arrow represents the observation plane which is imaged by imaging lens L2. (b) The tuneable beam displacer used to split the polarization speckles corresponding to x and y polarized light, the speckle field at distance z = 100 mm as shown by a green arrow location, is imaged by the tuneable beam displacer assembly at the detector

of the orthogonal polarization components is realized by the tuneable beam displacer as shown in Fig. 3.2(b). The overlap of the orthogonally polarized speckles is controlled by mirror M1 in the Sagnac geometry. This experimental design makes independent recording of orthogonally polarized speckles feasible from a single shot measurement.

3.4 Results and Discussion

In order to demonstrate reconstruction of the speckle free object, we consider four different cases of incident polarization. For each case, the speckle patterns are recorded with the CMOS camera. A random light field coming out of the tuneable beam displacer splits into

two orthogonally polarized components and is recorded simultaneously by the CMOS, as shown in Fig. 3.3.

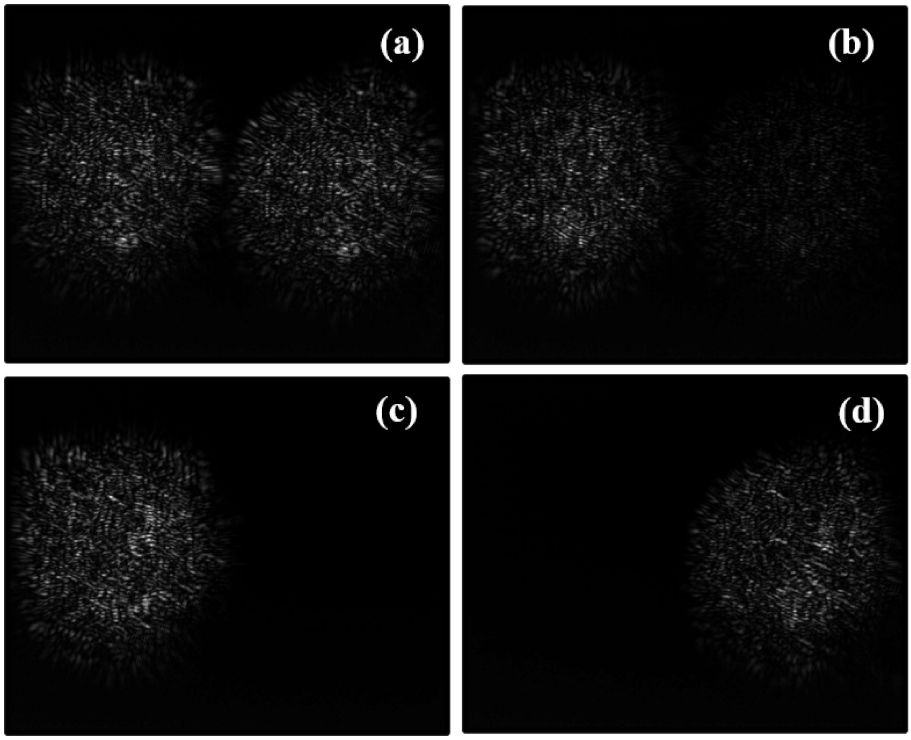

Fig. 3.3 (a) Speckle pattern for diagonally polarized light; both orthogonal polarization in one frame (b) speckle pattern for 60° polarized incident light (c) speckle pattern for x polarized light (d) speckle pattern for y polarized light

The speckle fields of the orthogonally polarized components for a diagonally polarized object beam are shown in Fig. 3.3(a). The object information is scrambled into the randomness and one of our objectives is to use these two random patterns to recover the polarization modes of the object. Similarly, speckle patterns of the orthogonal polarization components for a 60° polarized light are displayed in Fig. 3.3(b). The strength of the horizontal polarization component (x) is high in comparison to the vertical polarization component (y). Performance of our tuneable beam displacer is also tested for horizontal and vertical polarized incident fields and results are shown in Fig.s 3.3(c) and (d), respectively, for (x) and (y) incident polarizations. To quantitatively examine the performance,

we calculated the average value of speckle pattern intensity for (x) and (y) orthogonal polarization modes for incident horizontal and vertical polarized fields. For a horizontally polarized light, the average value of speckle intensity for the (x) polarization mode, is 28.37 times the average value of speckle intensity for the (y) polarization mode. Similarly, while measuring the speckle intensity for an incident vertically polarized field, the average value of speckle intensity for the (y) polarization mode, is 16.76 times the average value of speckle intensity for the (x) polarization mode. It is clearly seen that the strength of polarization speckles depends on the orthogonal components. For statistical analysis of these two orthogonally polarized components of the speckle patterns, we assigned 600×600 pixels for recording of the orthogonally polarized speckle out of 1024×1280 of the CMOS. Residual existence of the speckle noise can be removed by taking many measurements with independent speckles by either rotating the diffuser or sliding it. Here, we present fringes in the intensity correlation by utilizing 45 independent random patterns for a transparency and utilized 600×600 pixels of speckle pattern recorded at detector plane. These results are presented in Fig. 3.4 for different incident polarization state, and formation of the fringes in the intensity correlation is explained by Eq. 3.17.

Digital evaluation of the cross-covariance from the experimentally measured intensities is obtained by replacing ensemble averaging with space averaging under the condition of spatial stationarity and ergodicity as explained in theory section. This is implemented by picking a matrix of 200×200 pixels (shown as $I^n(r_x, r_y)$) from the 600×600 pixels of recorded intensity speckle. For the different realizations of random patterns, the cross-covariance can be given as, $\sum_{n=1}^{N} \frac{\Delta I(0,0)\Delta I^n(r_x,r_y)}{N}$, where N is the number of realizations which are obtained by pixel-by-pixel movement of matrix $I^n(r_x, r_y)$ over entire speckle pattern of 600×600 pixels. Here a two-dimensional scanning of matrix $I^n(r_x, r_y)$ over 600×600 pixels of resultant speckle pattern provides 400×400 different spatial realization. Analysis of one such speckle pattern gives the correlation fringes for a particular state of

polarization. Fig. 3.4 represents the correlation fringes for number “2”, where (a) and (b) are the x and y polarization components for a diagonally polarized light beam. Fig. 3.4(c) and 3.4(d) represents x and y, orthogonal polarized components for a 60° polarized light where strength of the y component is smaller than the x component as expected from corresponding speckle in Fig. 3.3 (b).

Experimental test is also conducted for pure orthogonal polarization components to check polarization leakage in tuneable beam displacer, and results in Fig. 3.4(e) and 3.4 (f) highlight that our beam displacer is capable to fully distinguish and separate the speckle patterns of the orthogonal polarization components. These results are obtained from the speckle patterns shown in Fig. 3.3(c) and 3.3(d) for x and y polarization components, respectively. A fast Fourier transform of these correlation fringes provides the reconstruction of transparency. The quality of reconstruction increases by adding more incoherent random patterns. In order to examine the effect of addition of more incoherent random patterns, we have evaluated the visibility for 1,10,20,40 and 45 incoherent patterns. The reconstruction visibility of an object is determined by how well it can be separated from background noise. Ratio of average image intensity of signal and average background image intensity provides the value of visibility [39]. Using this definition, we calculated visibilities for different cases. Evaluated visibility for 1,10,20,40 and 45 incoherent random patterns are 4.16,6.36,7.13,8.09 and 8.25 respectively. Results in Fig. 3.5 highlight the reconstruction of the orthogonal polarization modes from a single recording of the CMOS (rather than the average of 45 patterns), where (a) and (b) are the x and y polarization components for a diagonally polarized incident light beam. Fig. 3.5(c) and 3.5(d) represent x and y, orthogonal polarized components for a 60° polarized incident light beam. On the other hand, Fig. 3.5(e) and 3.5(f) correspond to reconstructed modes for only horizontal and vertical incident polarized light respectively. Strength of the x polarized component in the reconstruction is greater by the order of 1.75 in comparison to the y polarized component

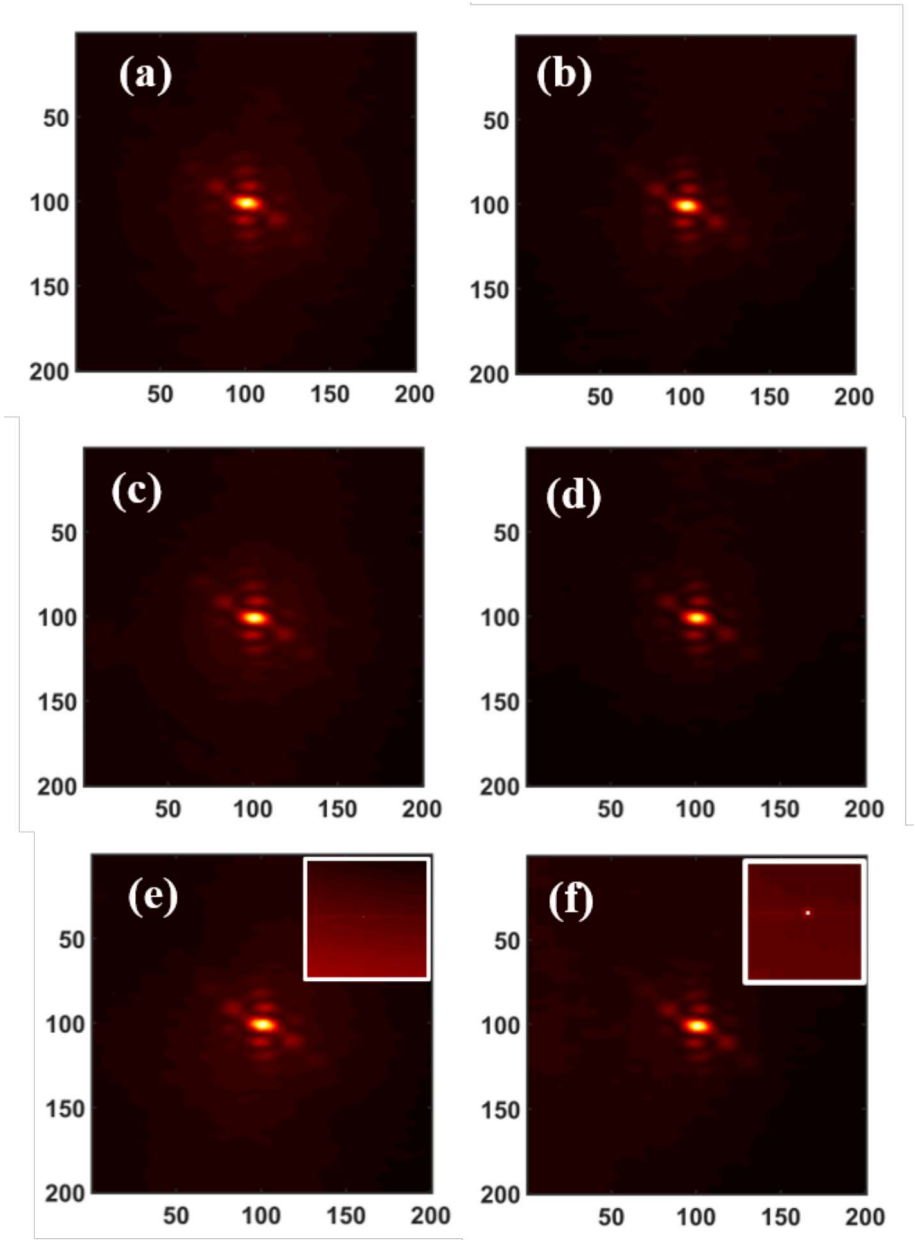

Fig. 3.4 Correlation fringes for number '2': (a), (b) for diagonally polarized incident light, (a) x polarized component, (b) y polarized component; (c), (d) for 60° polarized incident light, (c) x polarized component, (d) y polarized component; (e) for horizontally polarized incident light, x polarized component and inset in the right corner represents very weak y component ;(f) for vertically polarized incident light, y polarized component and inset in the right corner represents very weak x component.

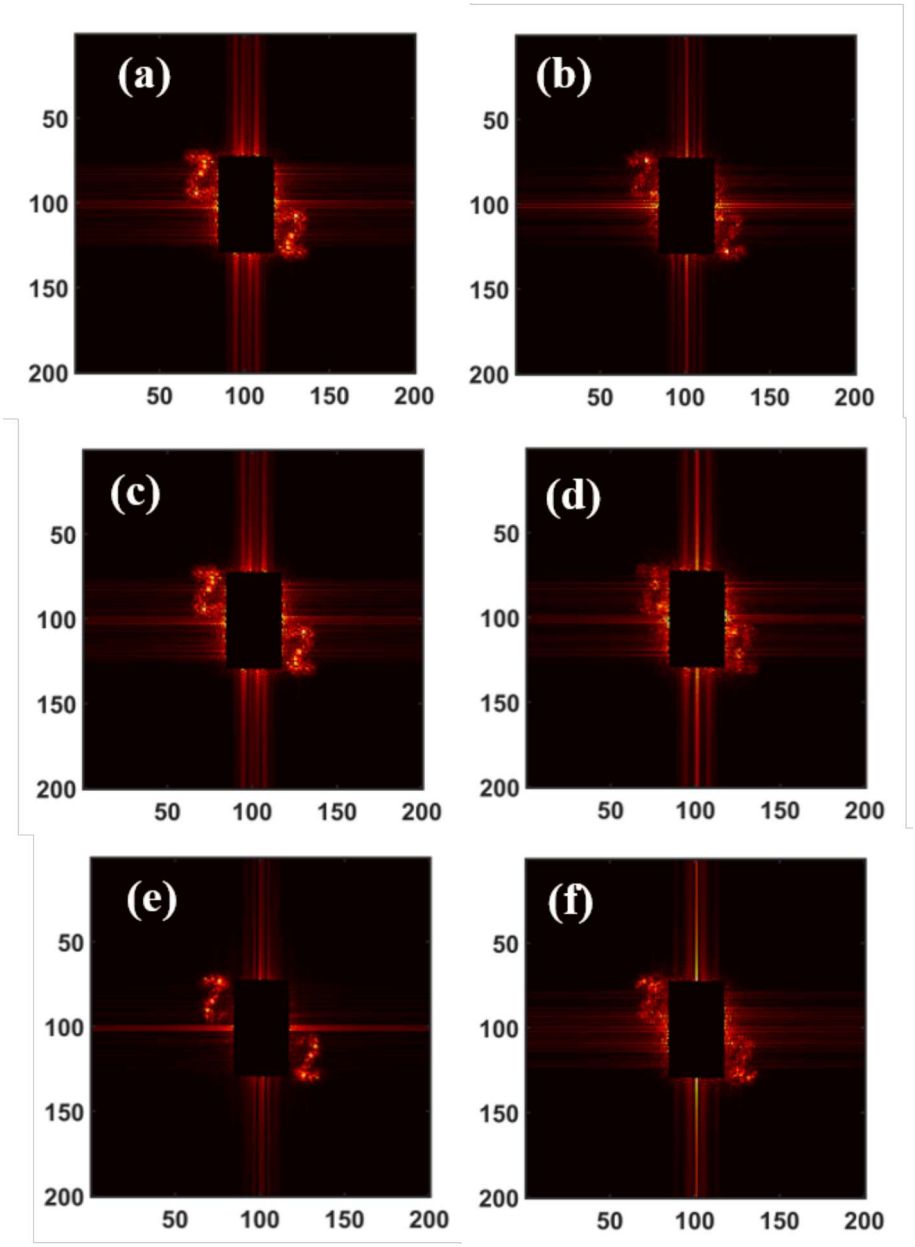

Fig. 3.5 Reconstruction of number '2': (a), (b) for diagonally polarized incident light, (a) x polarized component, (b) y polarized component; (c), (d) for 60° polarized incident light, (c) x polarized component, (d) y polarized component; (e) for horizontally polarized incident light, x polarized component; (f) for vertically polarized incident light, y polarized component.

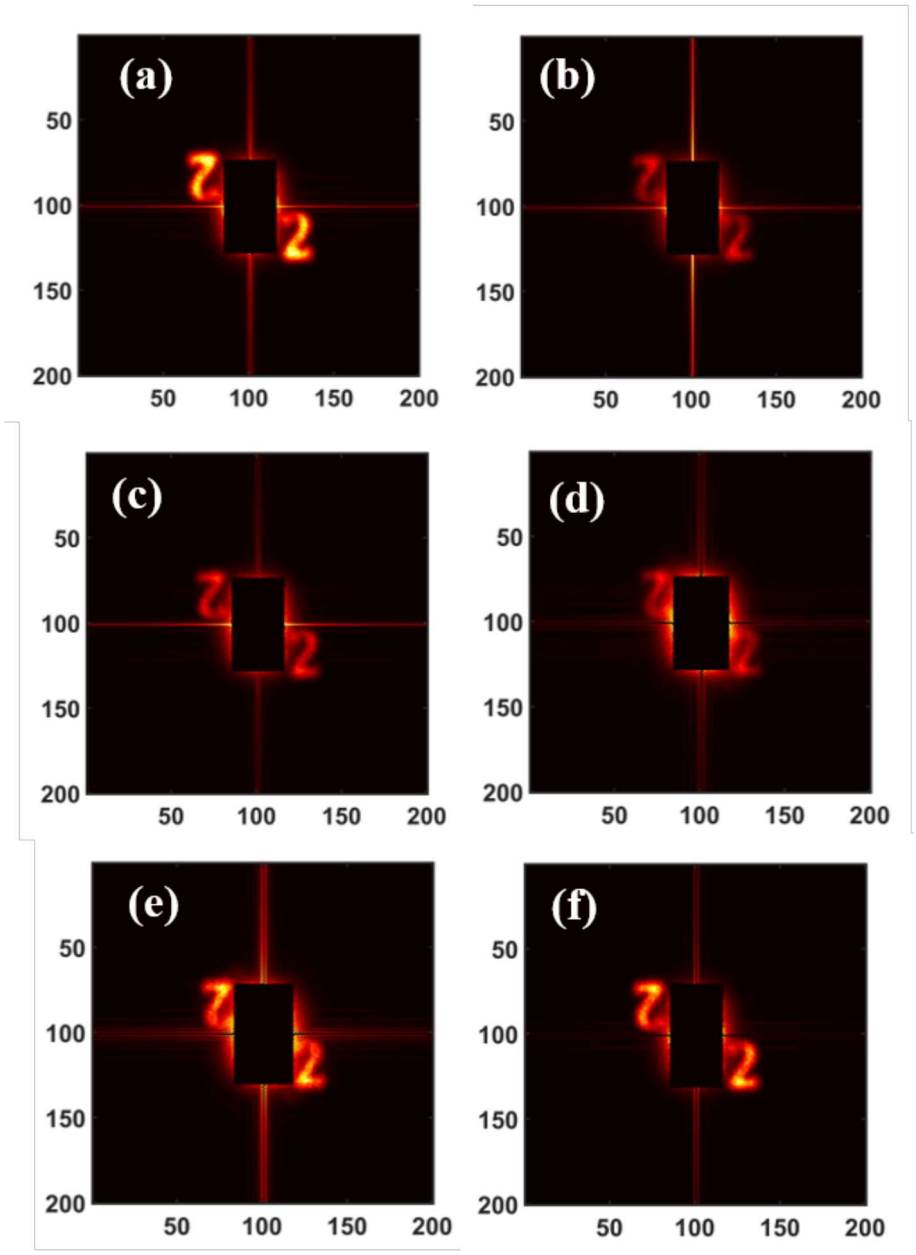

Fig. 3.6 Reconstruction of number '2' for incoherent addition of 45 random patterns: (a), (b) for diagonally polarized incident light, (a) x polarized component, (b) y polarized component; (c), (d) for 60° polarized incident light, (c) x polarized component, (d) y polarized component; (e) for horizontally polarized incident light, x polarized component ;(f) for vertically polarized incident light, y polarized component.

due to the polarization attenuation in the OHP sheet. This OHP sheet is used to print the object for display in experimental setup as shown by T.

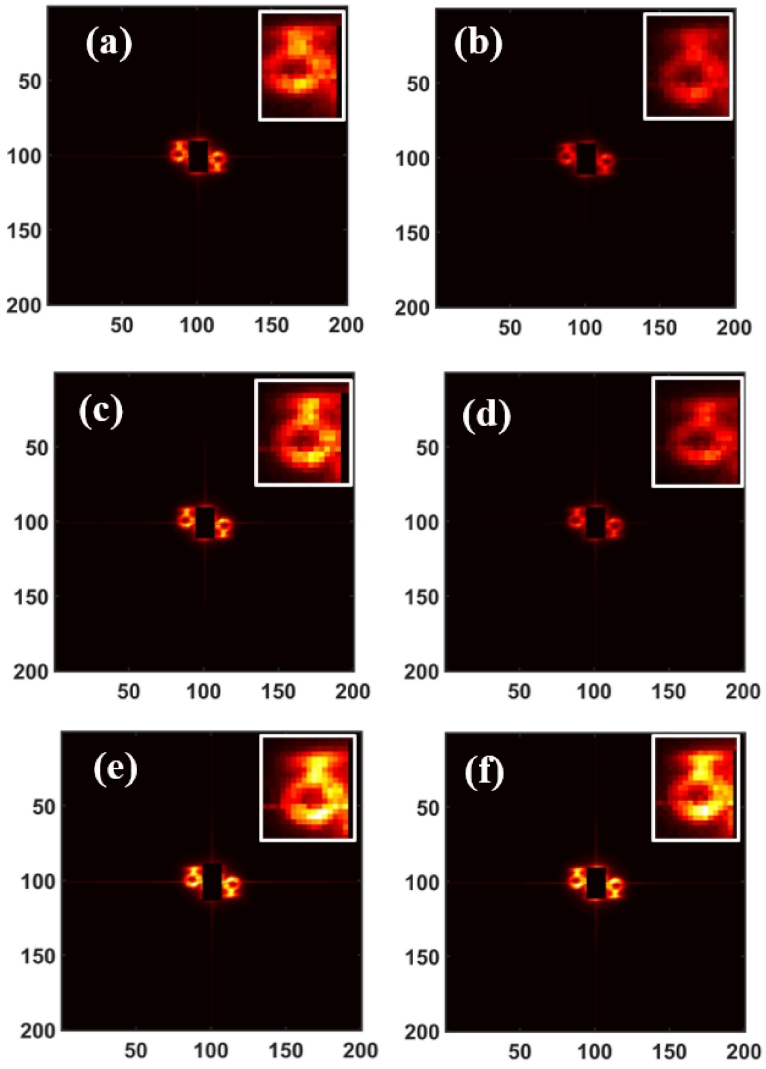

Fig. 3.7 Reconstruction of Hindi letter 'ठ ' for incoherent addition of 45 random patterns: (a), (b) for diagonally polarized incident light, (a) *x* polarized component, (b) *y* polarized component; (c), (d) for 60° polarized incident light, (c) *x* polarized component, (d) *y* polarized component; (e) for horizontally polarized incident light, *x* polarized component; (f) for vertically polarized incident light, *y* polarized component

To further remove randomness from the reconstructed object, as discussed in Fig. 3.5, we have used intensity correlation fringes with 45 incoherent random patterns by physically

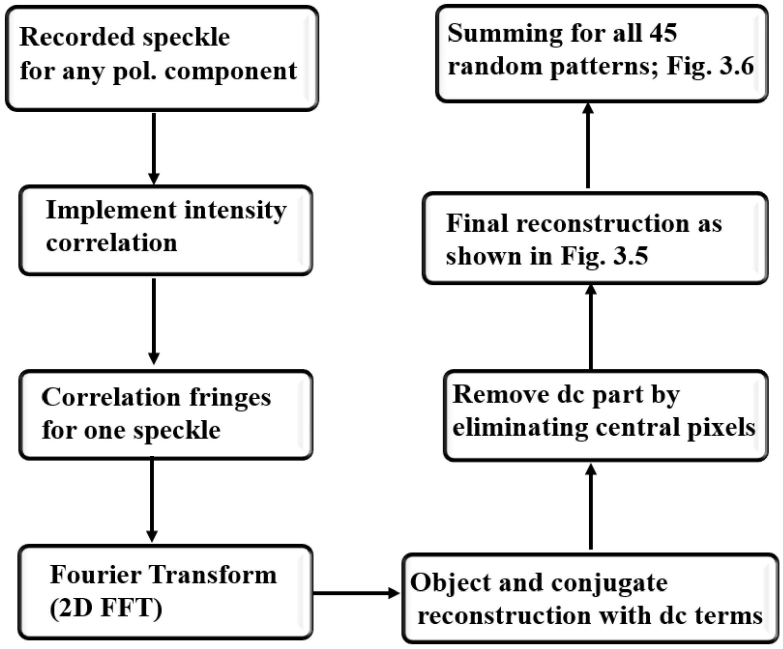

Fig. 3.8 Flow chart for the process of reconstruction of object from the recorded speckle

moving the ground glass 45 times. The correlation fringes are incoherently integrated for all 45 random patterns. Fig. 3.6 is the fast Fourier transform of intensity correlation for each incident polarization. The technique is verified by reconstructing two transparencies; numeric character "2" (size 2mm × 1.5mm) and Hindi letter "ठ" (size 1.4mm × 1mm), and the reconstructed results are shown in Fig. 3.6 and Fig. 3.7 respectively. In Fig. 3.6 and Fig. 3.7, (a) and (b) indicate the reconstruction of transparency for a diagonally polarized light beam, corresponding to both orthogonal polarization components. Similarly, (c) and (d) in Fig. 3.6 and 3.7 show the respective x and y polarized components for a 60° polarized light. Fig. 3.6 and Fig. 3.7, (e), and (f) show the reconstruction for incident horizontal and vertical polarizations, respectively. Magnified image is also shown in the top right-hand side in Fig. 3.7. A complete flow chart of retrieving object information from the recorded speckles is shown in Fig. 3.8.

3.5 Conclusion

In conclusion, we propose and experimentally demonstrate a new technique for simultaneous recovery of orthogonal polarization modes through diffuser. An edge referencing method for holography with the coherence waves is utilized for speckle free reconstruction of the orthogonal polarization modes. In order to tackle issue of the high scattering and intermixing of the speckles of the orthogonal polarization components, we designed a tuneable beam displacer with triangular Sagnac geometry. The experiment is performed for different states of polarization and results confirm suitability of our technique in the parallel recovery of polarization modes from the randomly scattered coherent light. Our proposed technique is expected to be useful in imaging, and retrieval of a hidden object from optically rough surfaces etc.